Journal of Fluids and Structures (2000) **14,** 103–125
doi:10.1006/jfls.1999.0254, available online at http://www.idealibrary.com on IDEAL®

AN INTEGRATED NONLINEAR APPROACH FOR TURBOMACHINERY FORCED RESPONSE PREDICTION. PART II: CASE STUDIES

M. Vahdati, A.I. Sayma and M. Imregun

Mechanical Engineering Department, Imperial College of Science Technology and Medicine, Exhibition Road, London SW7 2BX, U.K.

(Received 28 April 1998 and in final form 5 August 1999)

This paper discusses the application of an advanced turbomachinery forced prediction model to two representative turbomachinery cases: an HP turbine and a rig fan. The approach is based on an integrated nonlinear multi-passage analysis that includes both the stator and the rotor blade-rows. The numerical model has advanced features such as nonlinear friction damping for turbine blades, tip gap flows and blade vibratory motion. A series of inviscid and viscous computations were performed for an HP turbine with 36 stator and 92 rotor blades. The peak-to-peak maximum displacements were predicted with and without root friction dampers and the findings were compared with available experimental data. Good agreement was observed in most cases. It was found that most of the unsteady forcing was due to the potential effects. In a second phase of the turbine work, the response to low engine-order excitation was predicted using a multi-row whole-annulus model. The stator assembly was assumed to have blades with varying throat widths and the magnitude of the unsteady aerodynamic forcing was found to increase with increasing scatter in throat width variation. A second forced response study was conducted for a rig fan with 15 variable inlet guide vanes (VIGVs) and 20 rotor blades. For a 30° VIGV opening, a good match was observed between the predicted and measured wake profiles. Similarly, the measured and predicted rotor blade vibration levels were also found to be in good agreement. It is concluded that the proposed methodology can be applied, with reasonable confidence, to the study of industrial cases.

1. INDUSTRIAL REQUIREMENTS VERSUS CURRENT UNCERTAINTIES

High-cycle fatigue of turbomachinery blading due to forced response is one of the most serious problems for engine development and its avoidance is a primary industrial objective. Although Campbell diagrams are useful in indicating where resonances are likely to occur, they provide no information about the actual vibration levels for each resonance. On the other hand, designers need such data for assessing blade life. Currently, there are several uncertainties when determining the vibration levels, as follows.

(i) The harmonics present in the aerodynamic forcing, the so-called engine orders, are not necessarily well circumscribed. While the excitation from the upstream vanes and other obstacles is well defined in terms of blade numbers and their aliases, low engine-order harmonics arising from the general unsteadiness of the flow are much less understood.

(ii) The amplitude of the aerodynamic forcing at different engine-orders is difficult to predict.

0889–9746/00/010103 + 23 $35.00/0

(iii) The determination of the blade aerodynamic damping is not straightforward and it may be affected by the blade vibration itself.

(iv) The inherent structural damping is difficult to estimate under representative operating conditions. A mode-to-mode variation is likely, but usually unaccounted for.

(v) Nonlinear structural behaviour, due to friction dampers at blade roots and shroud interfaces, is very difficult to model accurately. Resonance shifts of up to 15% are observed in some cases.

(vi) Structural mistuning, i.e., small blade-to-blade differences due to manufacturing tolerances, will cause all blades to have different vibration amplitudes. A statistical analysis with large time-domain models is beyond available computational power.

In any case, the industrial requirement is to predict the blade vibration amplitudes to a given accuracy. Hence the case studies presented in this paper will focus on this specific issue.

2. FORCED RESPONSE STRATEGIES

The code AU3D, which is developed at Imperial College as part of a long-term turbomachinery aeroelasticity research programme, is based around the methodology described in Part I of this study (Sayma *et al.* 2000). Before conducting detailed case studies, it is proposed to outline the three forced response strategies that are available in AU3D. As will be demonstrated later, the code can be applied to any turbomachinery geometry, regardless of the rotor-to-stator blade ratio or the number and position of grid points in each domain. However, such a general approach is computationally very expensive and simplified representations are often needed for parametric design calculations.

2.1. Changing the Stator-to-Rotor Pitch Ratio

One possible simplification to avoid the computational expense associated with full multi-row models is to change the number of rotor blades. This approach allows the computations to be performed on a typical sector model of stator and rotor blades, and may allow a full viscous computation because of the reduction in the mesh size. For example, for a turbine with 40 stator blades and 92 rotor blades, one can use a ratio of $\frac{4}{9}$ by reducing the number of rotor blades to 90. Whereas such approximations have little effect on time-averaged pressure distributions, they may influence the temporal variations of the flow variables as well as far-field acoustics. On the other hand, by virtue of using a better discretization, the modified model is a more accurate representation of both wake and potential effects and it allows interactions between the stator and rotor blade rows.

2.2. Linked Single-Row Computations

In this approach, the steady-state viscous solution for a single stator passage is computed as a first step. The solution is then expanded for the whole stator annulus, so that it can be used as an inflow condition for the rotor. If there is no match between the blade numbers, the unsteady flow computations are performed in an inviscid or viscous fashion for a whole annulus; otherwise, a cyclic symmetry sector is used. With this approach, there is no need for altering the geometry or the number of the rotor blades, and both the wake and potential effects are modelled representatively. However, such an approach is not suitable for cases where the spacing between the stator and rotor rows is small, since no interactions are allowed between the rotor and the stator rows.

2.3. Multi-Row Computations

Linked single blade-row analyses remain valid provided that the two rows are set sufficiently far apart so that the interaction effects are minimal. However, the desire to reduce engine length requires the rotor and stator blades to be closely spaced, thus making multi-row analyses a necessity. The common approach used for modelling multi-row flows is to employ grids that move relative to each other. These grids are separated from each other by common boundaries, and the information is transferred from one grid to another by specifying appropriate conditions at these boundaries. As before, a representative sector may be used for matching rotor/stator blade numbers. If there is no match, whole-annulus models must be used, unless blade numbers can be modified at the expense of accuracy.

In any case, whole-annulus multi-row models are very general and can also deal with losses of symmetry which give rise to low engine-order excitation. The effects of structural mistuning can be analysed in a straightforward manner. However, a multi-stage viscous computation with whole-annuli requires very significant storage and CPU effort and cannot be undertaken for routine design calculations. An alternative approach is to use an inviscid flow representation plus a loss model to account for the viscous effects (Sayma *et al.* 1998). Such an approach may reduce the number of grid points by a factor of two and hence save significant computational effort. This particular route allows the potential effects to be modelled correctly, and provided that the loss model can produce a reasonable representation of the wake, these effects are also incorporated.

3. CASE STUDY 1: HP ROTOR

A high-pressure turbine with 36 stator and 92 rotor blades will now be studied in some detail. An industrial perspective and the results of a linearized flow analysis can be found in Green & Marshall (1999). Given the small axial gap, it was decided to perform a multi-row computation to include all possible interactions. In this case, a typical sector will consist of nine stator and 23 rotor blades and it was decided to reduce the computational effort by decreasing the number of stator blades to 90, thus allowing a ratio of $\frac{2}{5}$. The periodic boundaries were imposed only between the first and the last passages of each blade row.

3.1. Structural Model

The structural model of rotor blade, obtained using a standard FE package, is shown in Figure 1, together with the two modes of interest for the forced response calculations: first torsion (1T) and second flap (2F). In this study, it was decided to use a Q-factor[†] of 200 for the 1T mode and of 50 for the flap mode. However, it must be recognized that an accurate modelling of structural damping is at least as difficult as that of the aerodynamic damping and that different nodal diameter modes may well exhibit different structural damping characteristics.

3.2. Solution Procedure

Since the starting flow conditions are not known, it is desirable to reach a state for which the initial transients are no longer in the solution domain. Furthermore, as the aim is just to produce some (almost arbitrary) starting state, the calculation must be initiated in a manner

[†] Q-factor $= 1/\eta$, where η is the inherent structural damping due to the energy dissipation properties of the material.

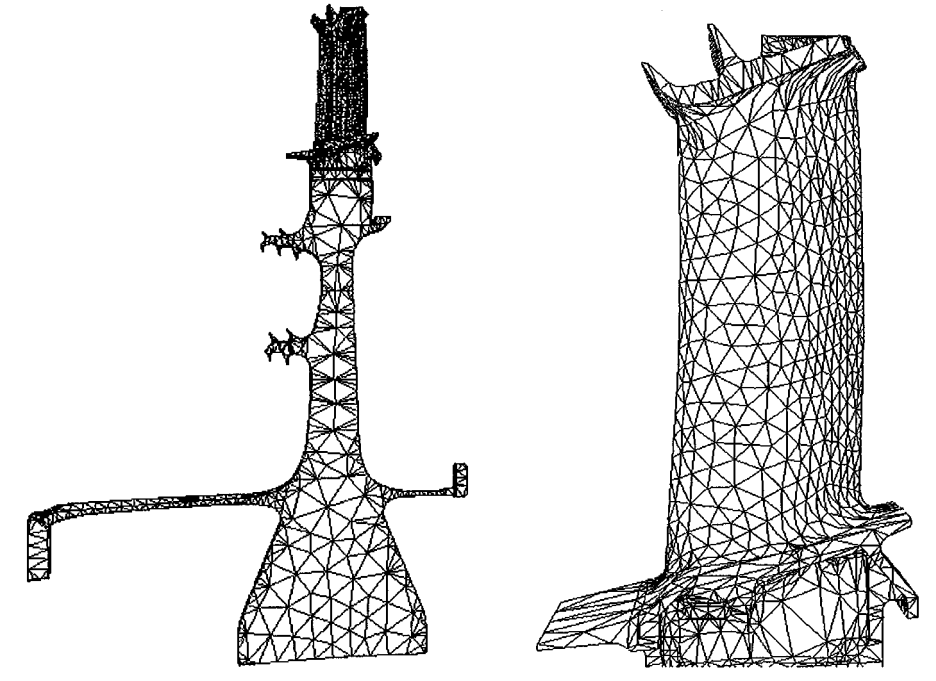

(a)

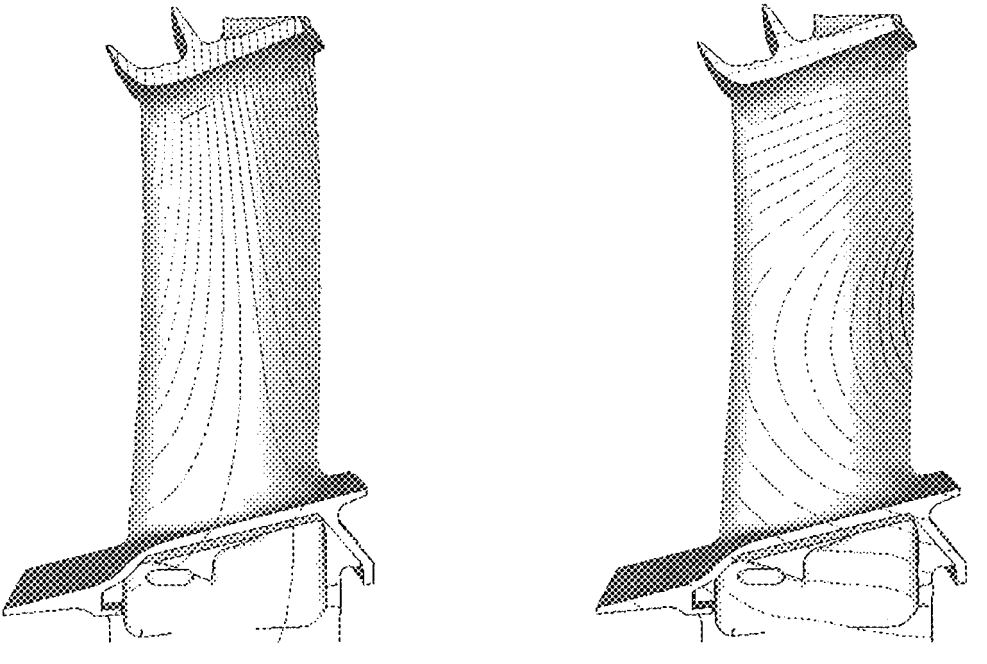

(b)

Figure 1. (a) FE model of the rotor blade. (b) Vibration shapes for 1T and 2F modes

which requires the minimum amount of computational time. This can be achieved as follows: (i) compute a single-stage steady flow for a single stator blade by using the available inlet and exit boundary conditions; (ii) compute a single-stage steady-state flow for a single rotor blade by using the available inlet and exit boundary conditions; (iii) expand the solutions of steps (i) and (ii) to form a typical two-stage sector; (iv) compute a multi-row steady-state flow for the typical sector by using the result of step (iii) an initial condition; this is the end of the start-up procedure; (v) proceed with the unsteady forced response calculations by using the results of step (iv) as a steady-state initial condition.

In the steady-state computations of steps (i)–(iv), the solution is integrated in time by using local time steps. This allows the mass flow to stabilize and the wake region to develop quickly. In the time-accurate computations of step (v), a minimum allowable time-step, based on the computational mesh, is used in the integration procedure.

3.3. Steady-Flow Predictions

As shown in Figure 2, the aerodynamic mesh of the stator blade is unstructured in the axial and tangential directions (i.e., the cross-sectional plane) and structured in the radial direction. It is easily seen that this semi-unstructured meshing approach allows one to obtain very good leading- and trailing-edge definitions without creating superfluous points elsewhere. The suitability of this type of semi-unstructured mesh to turbomachinery applications is demonstrated by Sbardella *et al.* (1997).

The Mach number contours of the viscous stator domain are shown in Figure 3. It can easily be seen that there is a circumferential nonuniformity in the nozzle passage, a feature which will lead to unsteadiness in the rotor frame. Broadly speaking, this nonuniformity can be decomposed into two parts: (a) a pressure nonuniformity which gives rise to a purely inviscid interaction, and (b) a velocity field (or wake) nonuniformity which is generated by the viscous effects. The rotor domain is treated inviscidly and such a simplification can be justified by remembering that, although the wakes are generated by viscous effects, their subsequent interaction with the stator blades is, in the main, an inviscid process. The inviscid computational mesh and a solution for the steady-state flow are shown in Figure 4.

3.4. Aeroelasticity Calculations

The rotor/stator calculations were performed in a coupled fashion in which the flow variables and the displacements are advanced in time simultaneously by exchanging boundary conditions. Consequently, features such as fluid damping and blade motion are modelled automatically. In order to differentiate between the potential and wake effects, the stator domain was modelled via both inviscid (173 000 points) and viscous (305 000 points) meshes which are plotted in Figure 5(a). A 3-D view is shown in Figure 5(b). Contour plots of the instantaneous static pressure and of entropy are shown in Figure 6 for some arbitrary time instant. It is immediately seen that the wakes and the shock waves pass through the interface boundary without any distortions, indicating the success of the interpolation scheme. It is also seen that there is a strong interaction between the stator blade shocks and the rotor blades. The oblique shock extending downstream of the trailing edge of the upper stator blade interacts with the expansion region near the leading edge of the second rotor blade, causing the shock wave strength to decay. At a later time, this shock will hit the crown of the suction surface of the third rotor blade, causing large variations of pressure on this blade. It is apparent that, as a result of shock–rotor interaction, the largest variation of rotor surface pressure occurs in the vicinity of the leading edge. Also, as can be seen from the instantaneous rotor static pressure profiles of Figure 7, there is a considerable temporal

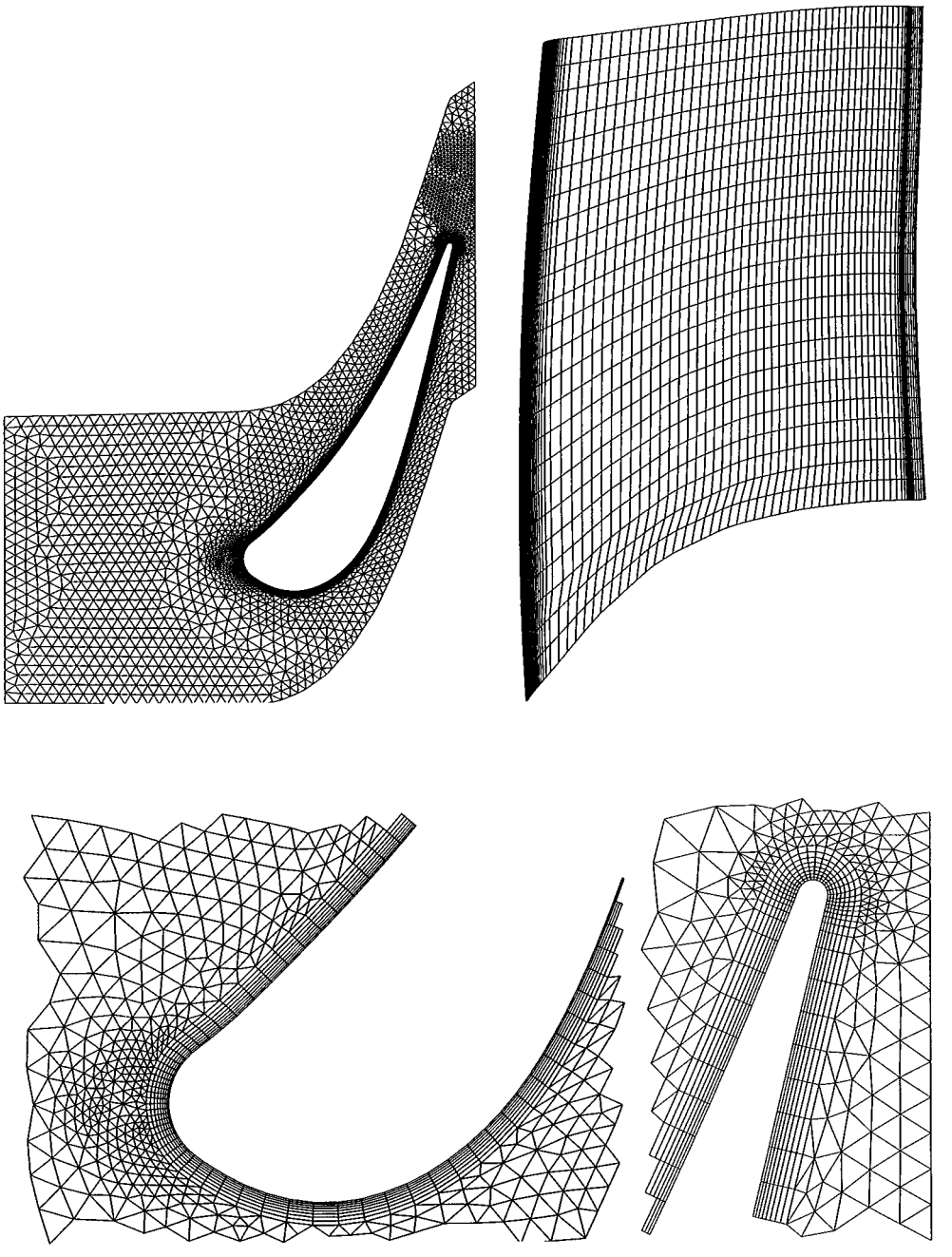

Figure 2. Mesh for the stator blade.

variation in the pressure profile around the rotor blades and a significant movement of the shock. An inspection of the modal time histories for the first four blade modes reveals that only the 1T mode contributes to the response since the aerodynamic condition used corresponds to this particular resonance. A comparison of the viscous and inviscid stator

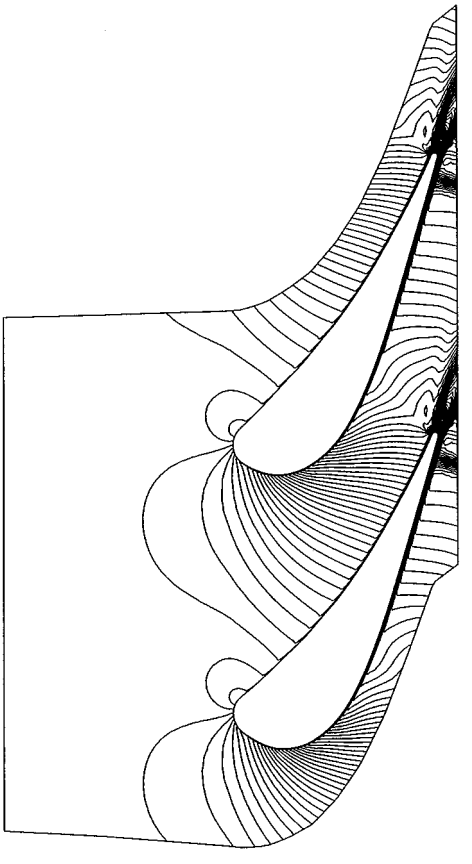

Figure 3. Mach number contours of the viscous stator domain.

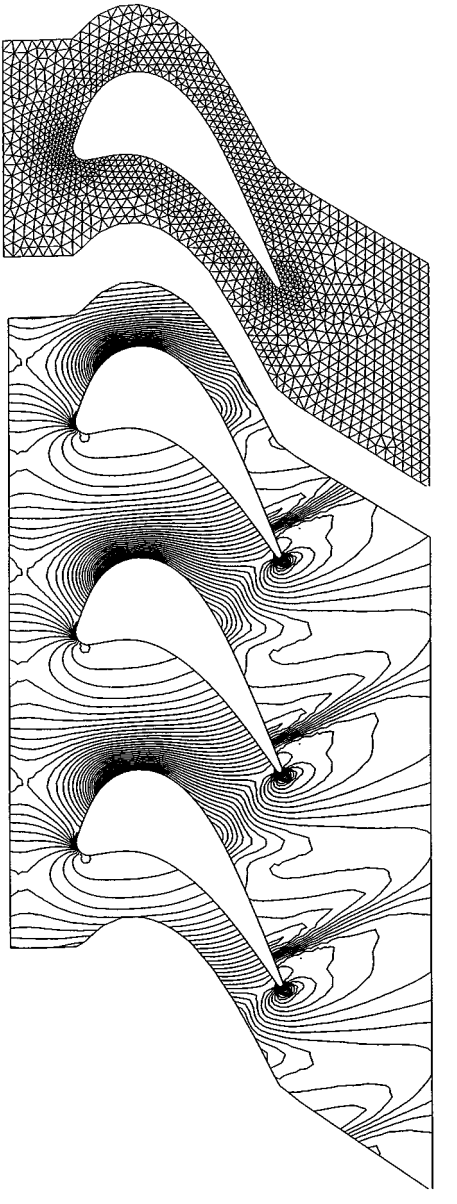

Figure 4. Computational mesh and the steady-state flow for the rotor blade.

domain calculations is shown in Figure 8. It is seen that about 85% of the modal forcing is due to potential effects and that the (viscous) wake effects are responsible for the remaining 15%. The actual time history at the trailing edge of the shroud is shown in Figure 9. For this viscous calculation, the peak-to-peak amplitude is seen to be 0·28 mm. The corresponding inviscid computation yielded a peak-to-peak amplitude of 0·21 mm.

The effect of fluid damping was investigated by switching the blade motion off and re-computing the modal forces. A comparison of the modal forces is given in Figure 10 and

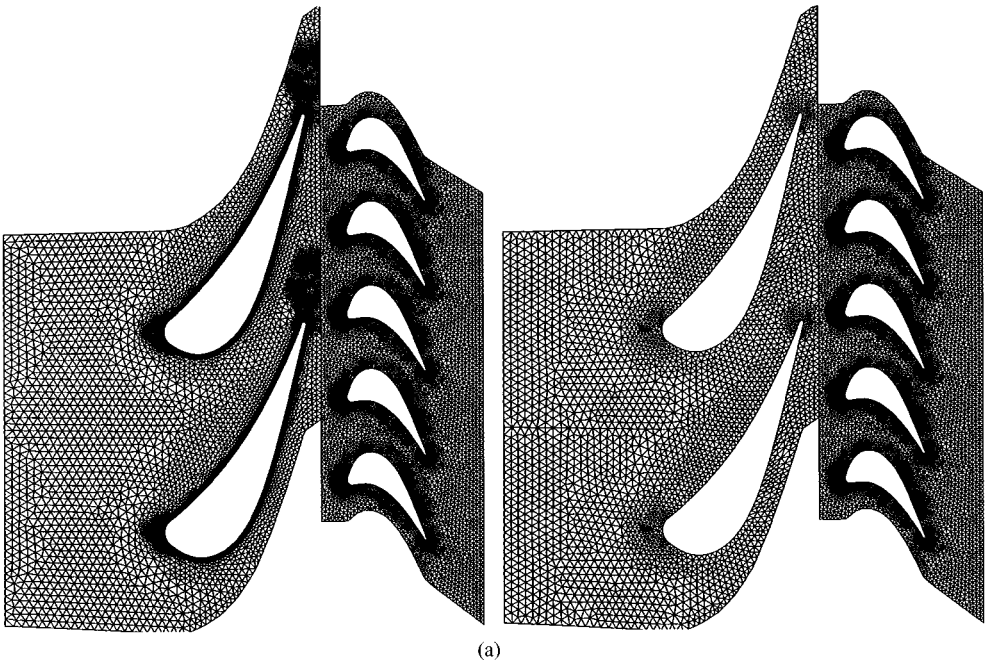

(a)

(b)

Figure 5. (a) Viscous and inviscid meshes for a typical sector (rotor mesh is inviscid in both cases), and (b) 3-D view of the rotor/stator mesh.

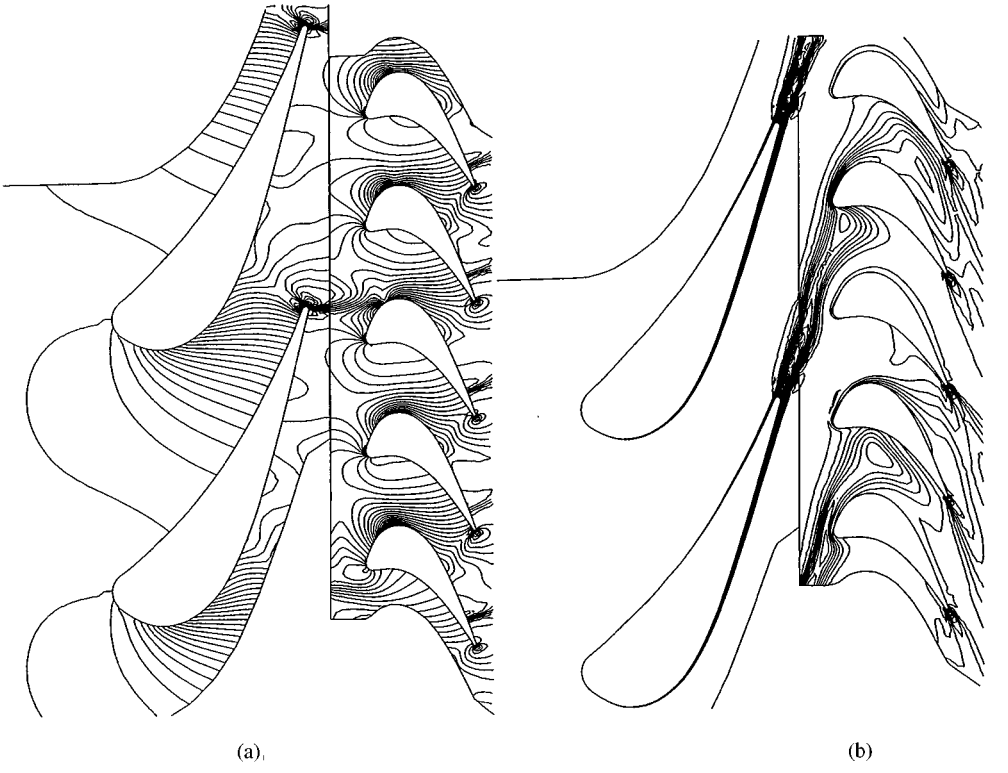

Figure 6. (a) Contour plots of the rotor instantaneous static pressure, and (b) contour plots of the instantaneous rotor entropy.

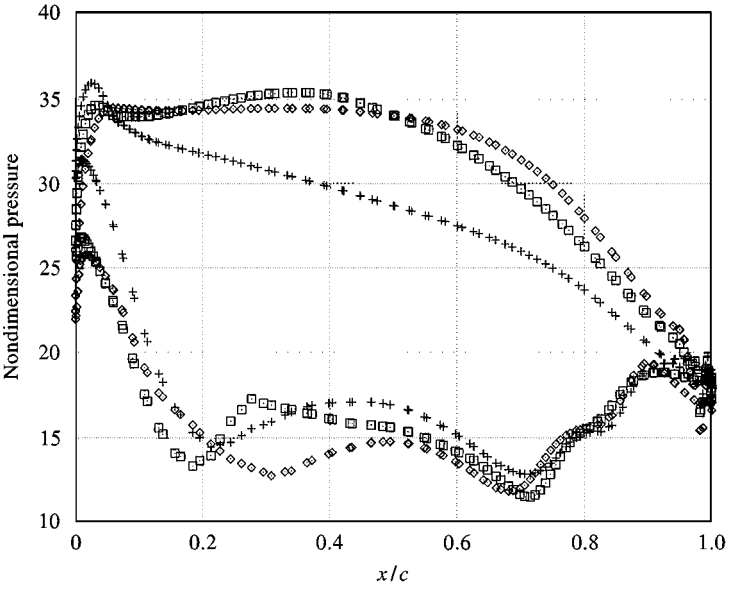

Figure 7. Instantaneous rotor static pressure profiles.

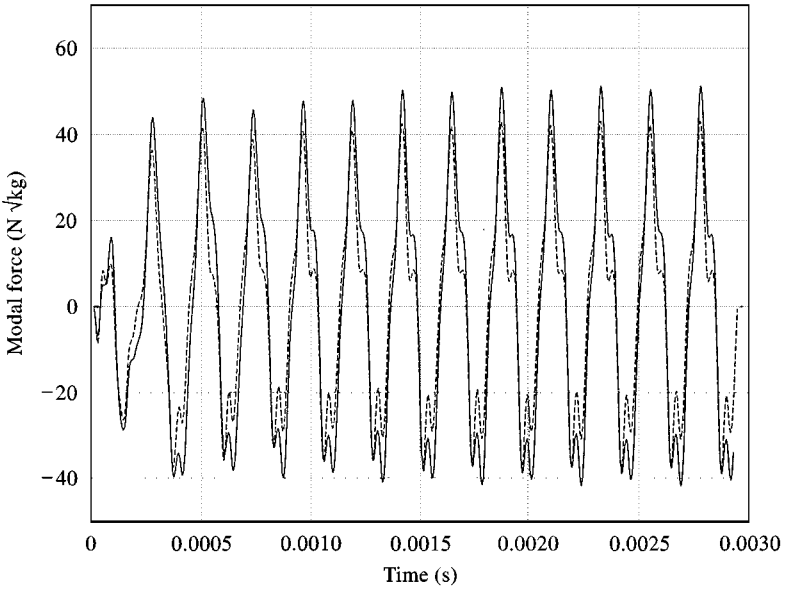

Figure 8. Modal forces obtained from viscous and inviscid stator representations: viscous —, inviscid – – –.

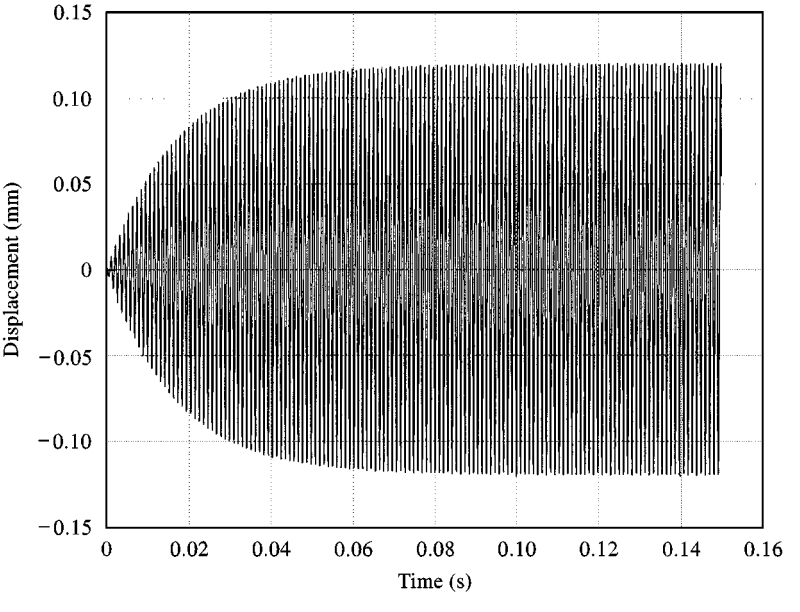

Figure 9. The actual time history at the trailing edge of the shroud.

it is seen that the differences are small, indicating that the fluid damping has a small effect in this particular case.

3.5. Inclusion of Friction Dampers

A one-dimensional friction damping model, developed by Sanliturk *et al.* (1996), was used to investigate the additional damping effects. The dampers were placed between the adjacent

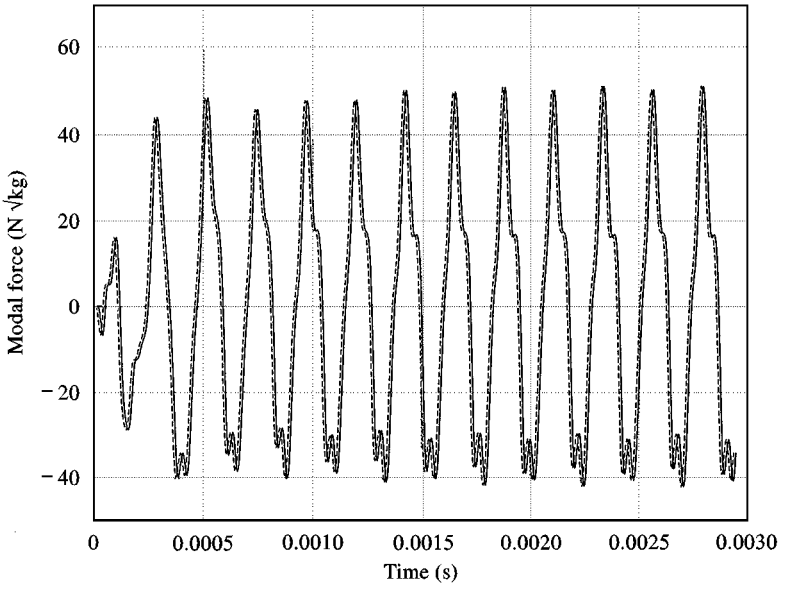

Figure 10. Modal forces obtained from coupled and uncoupled analyses: ——, uncoupled; – · – · –, coupled.

blades at the root and were connected to one point on each blade, each opposing the motion along the line joining the two blades. The parameters of the friction damper were determined experimentally to match the particular rotor blade under study. As the friction dampers are likely to change the resonant conditions, the computations would need to be performed using a sweep in speed. However, not only is it impractical to use a nonlinear time marching code in this fashion, but also a new aerodynamic condition would be needed at each speed. It was decided to obtain the aerodynamic forcing at three conditions (reference excitation frequency, + 10% and − 10%) and the forcing at the remaining frequencies was obtained via linear interpolation or extrapolation from these three conditions. In any case, the computed force–displacement characteristic is shown in Figure 11 for the 1T mode. The amount of energy dissipated can be calculated from the area of the hysteresis loop.

3.6. Comparison with Experimental Data

The forced response results are summarized in Table 1 where the findings for the 2F mode are also summarized. It is easily seen that the vibration amplitude is predicted with very good accuracy when there are no friction dampers. The discrepancy between the measured and predicted results is much larger when the friction dampers are included. This is thought to be due to the limitation of the damper model which considers a line contact mechanism only. Also, the coefficients of the model are based on experimentally derived values obtained under laboratory conditions and may not be representative of true operational behaviour.

3.7. Effect of Reducing the Number of Rotor Blades

For the same operating conditions, the effect of reducing the number of rotor blades was investigated by modelling the exact blade numbers using a much larger typical sector

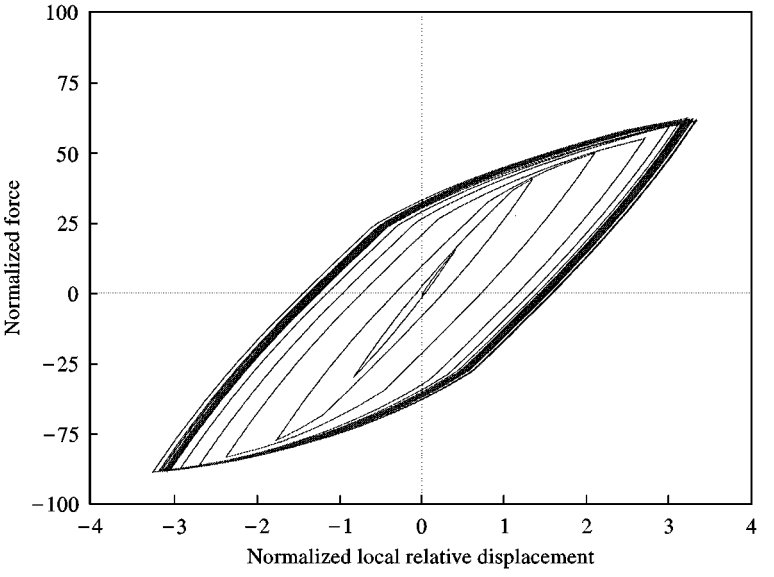

Figure 11. Predicted hysteresis loop for the friction damper for 1T mode.

TABLE 1

Measured and predicted peak-to-peak vibration amplitudes (FD: friction damper)

Case	Predicted amplitude (mm)	Measured amplitude (mm)
1T mode	0·28	0·28
1T mode with FD	0·14	0·09
2F mode	0·11	0·12
2F mode with FD	0·08	0·04

consisting of 23 stator and 9 rotor blades. The main aerodynamic and aeroelastic findings were found to remain unchanged. It was also observed that the peak-to-peak amplitude was reduced by 5% when all 92 blades were modelled.

3.8. Study of Low Engine-order Excitation

As discussed in Part I, one particular regime of forced response, which can occur at much lower frequencies than the blade-passing frequency, is the so-called low engine-order (LEO) forced response. The unsteady aerodynamic forcing that causes LEO forced response is called LEO excitation, the creation mechanism of which is much more complex than that for blade-passing forced response. The source of the LEO excitation is largely unconfirmed but it is believed that some loss of symmetry, such as inherent nonuniform spacing of the stator blades, is the most probable cause. However, many other factors, such as flow exit angle variations, rotor–stator axial gap differences, combustion effects such as burner blockages and nonuniform temperature distributions, combinations of blade numbers,

Figure 12. Multi-stage whole-annulus model for low-engine-order calculations.

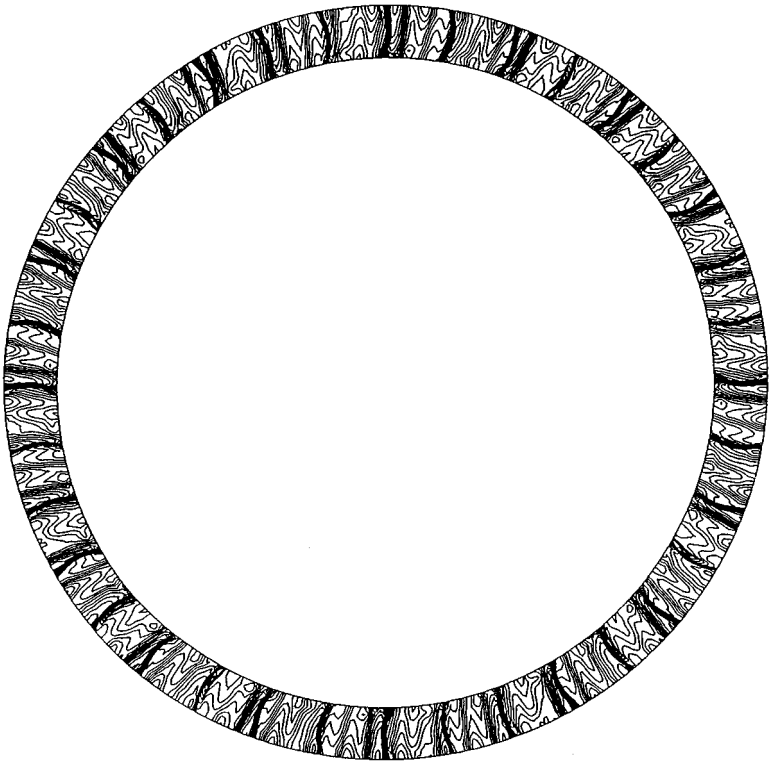

Figure 13. Unsteady pressure field at the stator outflow.

effects of downstream and upstream stages, can also influence the LEO excitation mechanism.

Here it is proposed to focus on the throat-width variation of the stator blades. Although this variation is random in practical situations, a well-defined pattern was used here by generating eight pairs of passages with a larger throat width, these being separated by two or three standard passages. This arrangement is expected to produce 4th and 8th engine-order excitations and the aim is to relate the strength of the ensuing aerodynamic forces to the imposed throat width variation. Three cases of 1, 3 and 5% variation were considered. Clearly, such a study can only be conducted using a multi-row whole annulus model, an inviscid mesh of which is shown in Figure 12. The pressure field at the stator outflow is shown in Figure 13 for the 3% variation case. A Fourier transform of the pressure distribution along a circumferential line at constant radial distance is plotted in Figure 14 for all three cases and, as expected, 4th engine order and its higher harmonics are present in the unsteady pressure distribution. Finally, the time history of the resulting modal displacements is plotted in Figure 15. The modal displacement amplitude is seen to increase with increasing throat width.

4. CASE STUDY 2: FAN FORCED RESPONSE

The second case study is focused on a research fan rig with variable inlet guide vanes (VIGVs) which articulate from 5 to 70° (Edmonds *et al.* 1997). The rotor is a blisk with 20 blades while there are 15 VIGVs. The fan is known to have two very close resonant

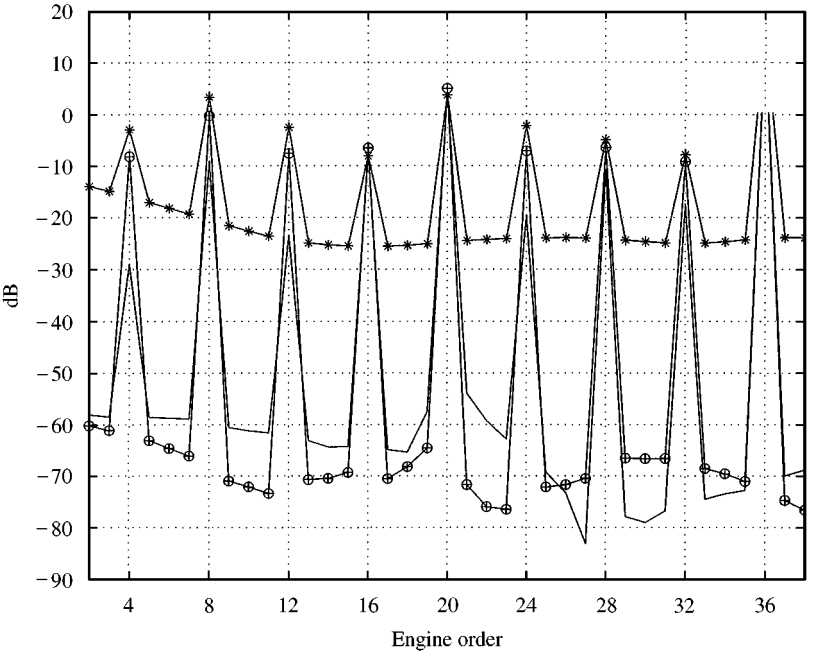

Figure 14. Fourier transform of the unsteady pressure distribution at the stator outflow: ——, 1% variation; —◦—, 3% variation; —∗—, 5% variation.

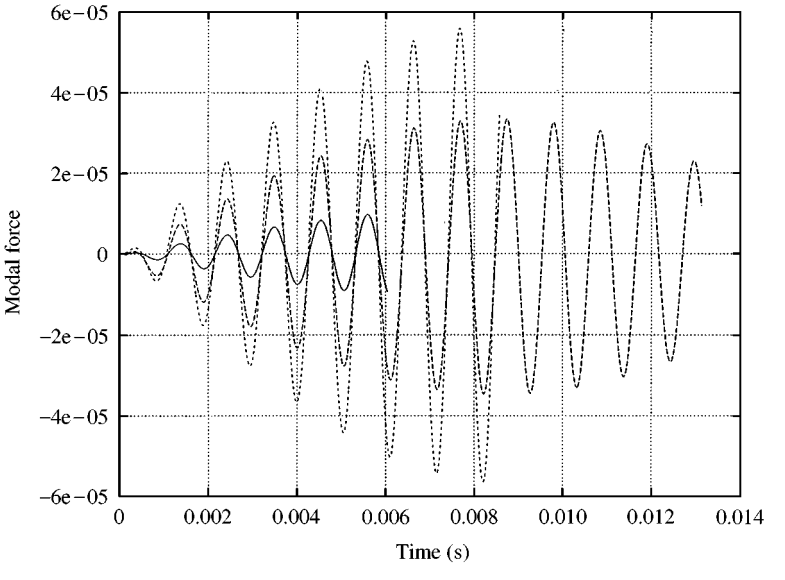

Figure 15. Variation of modal displacement amplitude with throat width: ——, 1% variation; – – – –, 3% variation; - - - -, 5% variation.

conditions due to 15 VIGV wakes exciting two close assembly modes of the 20-bladed rotor, the assembly modes arising from blade modes 11 and 12. Both resonances occur in 5-nodal-diameter modes because of the aliased five engine-order excitation on the rotor blades. The exact match between blade numbers allows the use of a typical sector with

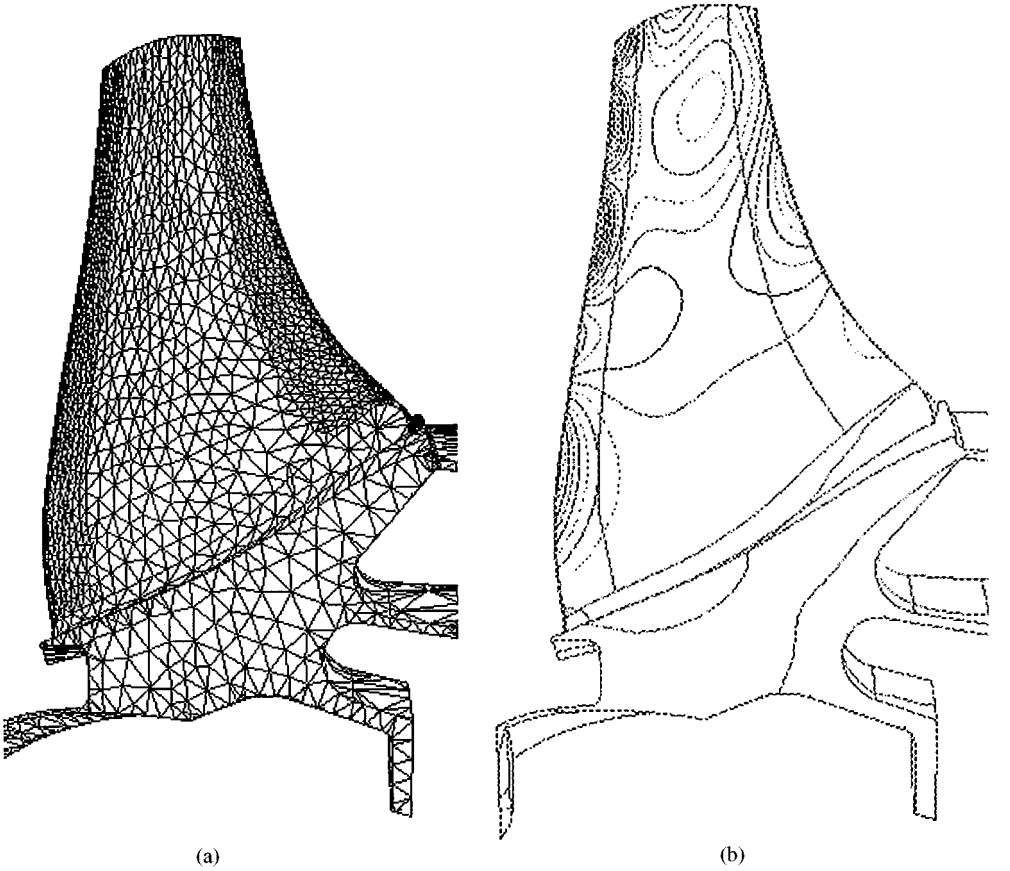

Figure 16. FE model for the fan blade and mode shape for mode 12.

3 VIGVs and 4 rotor blades, an arrangement which also happens to accommodate the 5-nodal-diameter pattern. The structural analysis was performed using a standard FE code and cyclic symmetry. The rotor blade mesh is shown in Figure 16(a), while the mode shape for blade mode 12 is shown in Figure 16(b).

From the outset, it was decided to conduct the flow analysis in a viscous fashion as the correct determination of the shock position is essential for fan blades. Semi-structured meshes were generated for single-passage 30° VIGV and fan blade domains using about 160 000 and 120 000 grid points, respectively (Figures 17 and 18). A tip gap mesh was included for the VIGV but the flow through its middle hinge was not modelled. For the part-speed of interest, the Mach number contours near the tip of the VIGV are shown in Figure 19. It can be seen that there is significant swirl near the tip, a feature that can only be detected with a tip gap. Calculations without a tip gap model, not reported here, were unable to reproduce the swirl, the presence of which is confirmed experimentally (Edmunds *et al.* 1997). The measured and predicted 30° VIGV wakes are plotted in Figure 20, and it is seen that the agreement is good at all three spanwise locations. Similarly, a steady-state solution was obtained for the fan blade and the Mach number contours near the VIGV exit are shown in Figure 21.

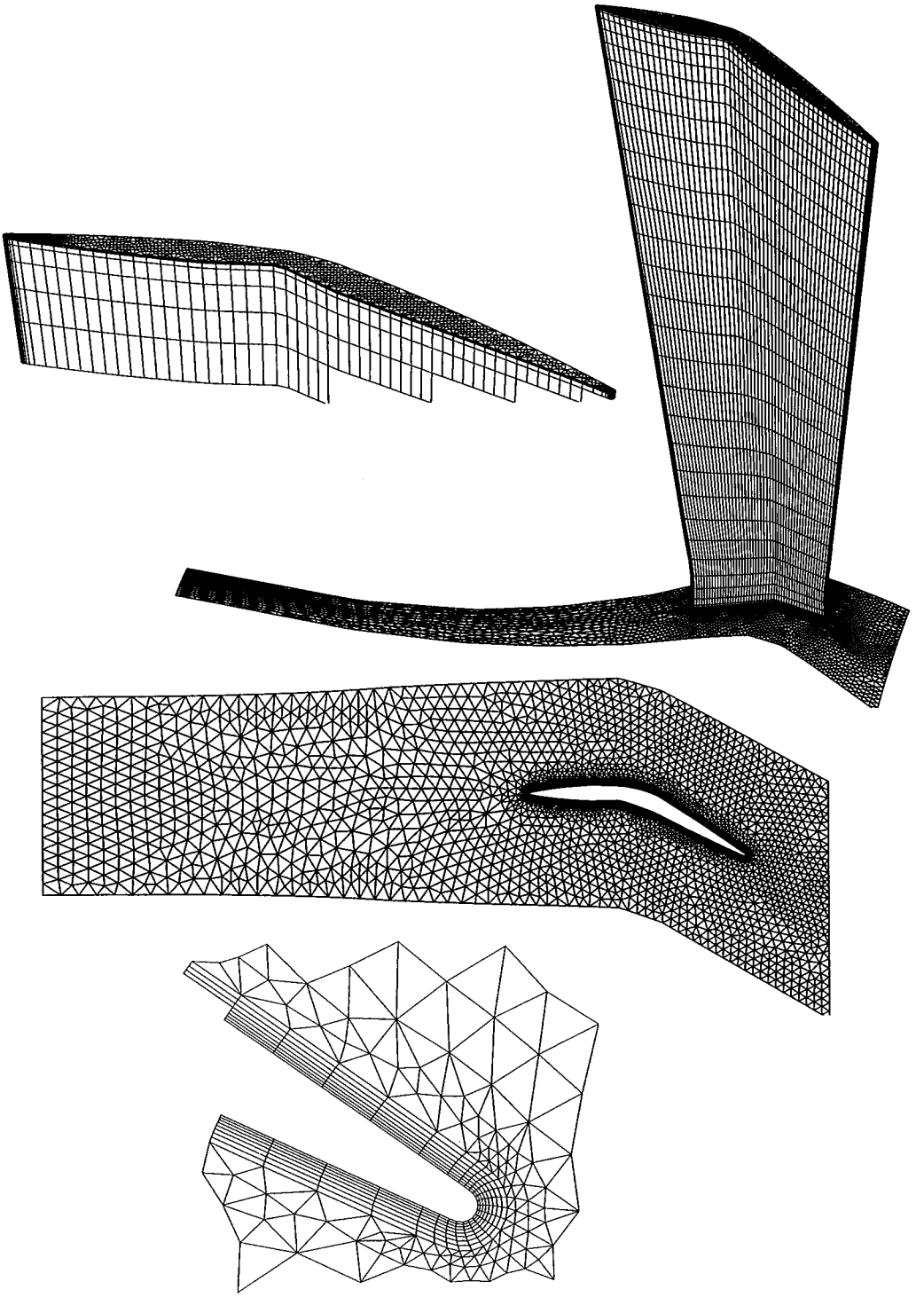

Figure 17. Single-passage viscous mesh for 30° VIGV.

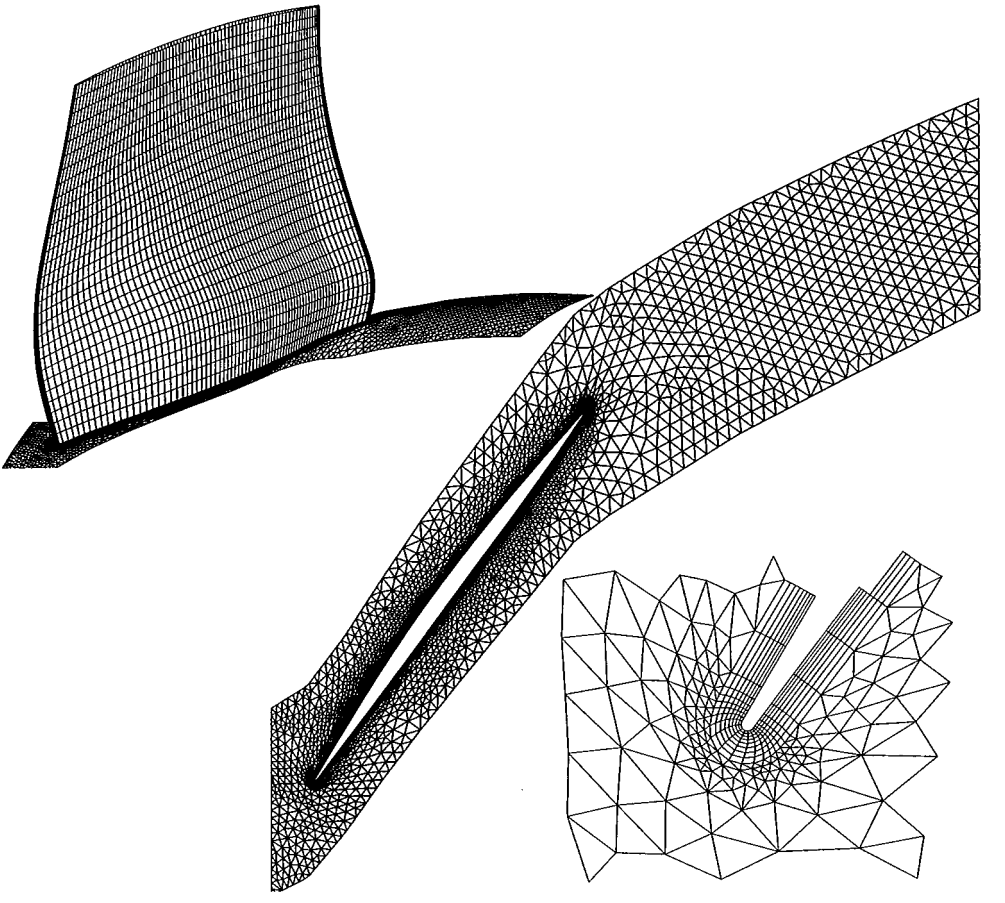

Figure 18. Single-passage viscous mesh for fan blade.

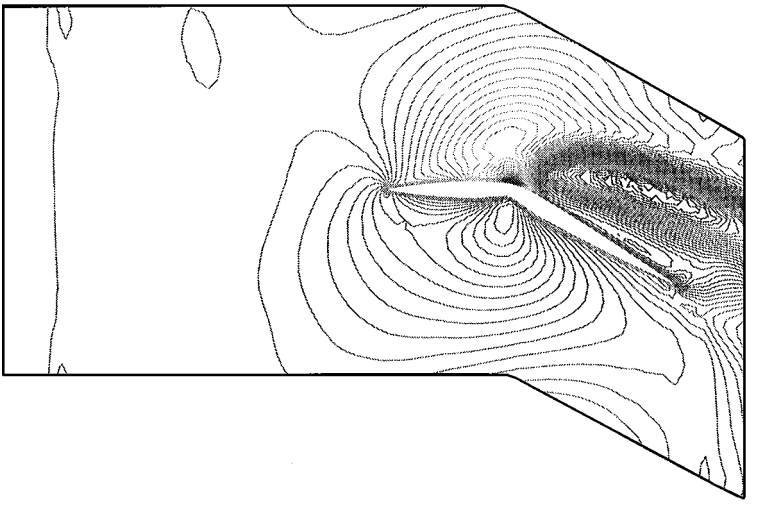

Figure 19. Mach number contours near VIGV tip.

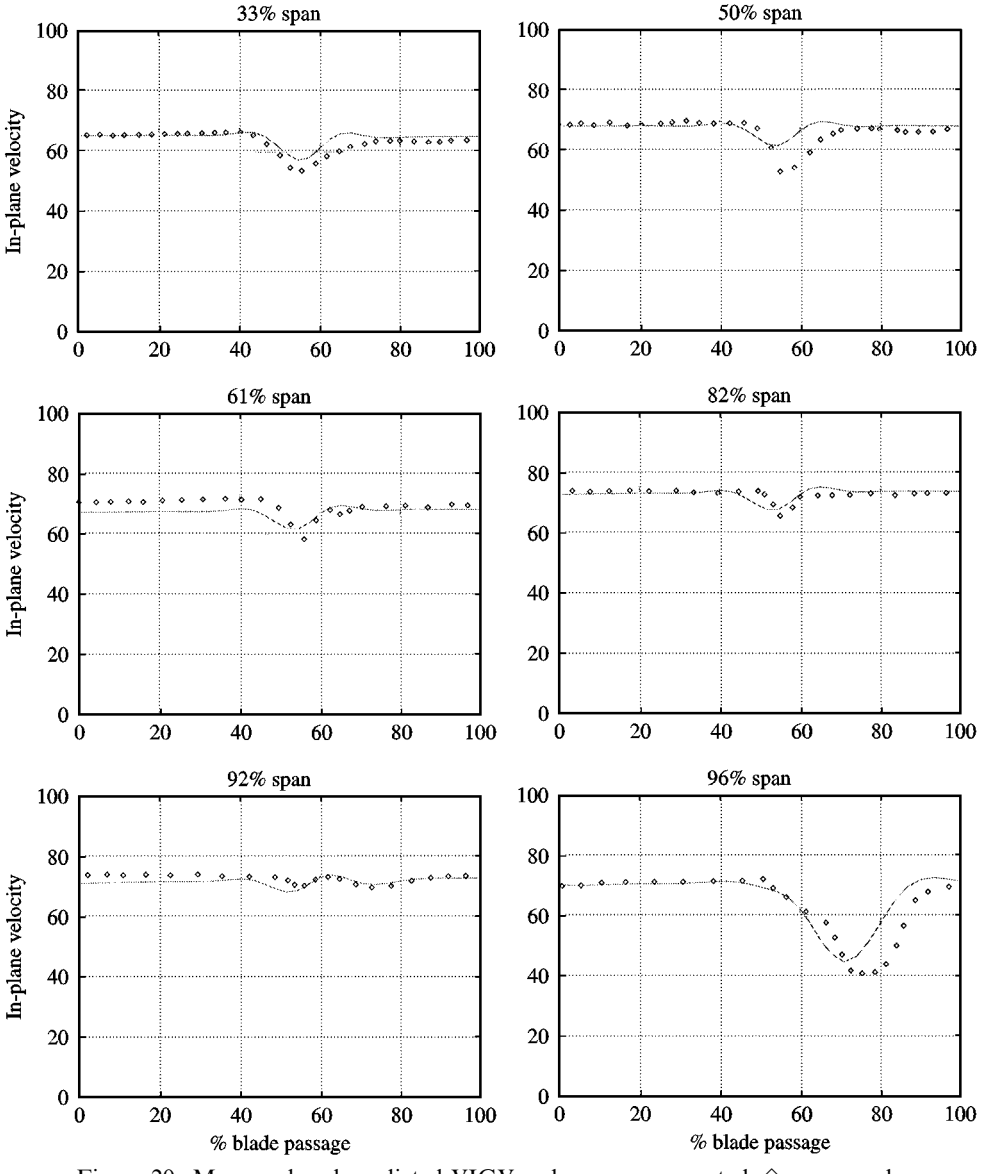

Figure 20. Measured and predicted VIGV wakes: ....., computed; ◇, measured.

Forced response predictions at a part-speed, corresponding to the two resonances of interest, were performed next. The multi-row sector mesh, shown in Figure 22, was assembled from the individual single-passage meshes and contained about 1 000 000 grid points. The two single-passage steady-state solutions were used as a starting condition for the viscous time-accurate unsteady computations with blade motion. The values of inherent structural damping were based on available experimental data . The instantaneous pressure and Mach number contours are shown in Figure 23. Compared to the steady-state solution, the shock position on the rotor blade is seen to be significantly different, a feature which is due to both potential flow variations and VIGV wake effects. In any case, the aerodynamic excitation on the rotor blades is predicted in the form of modal force time histories which

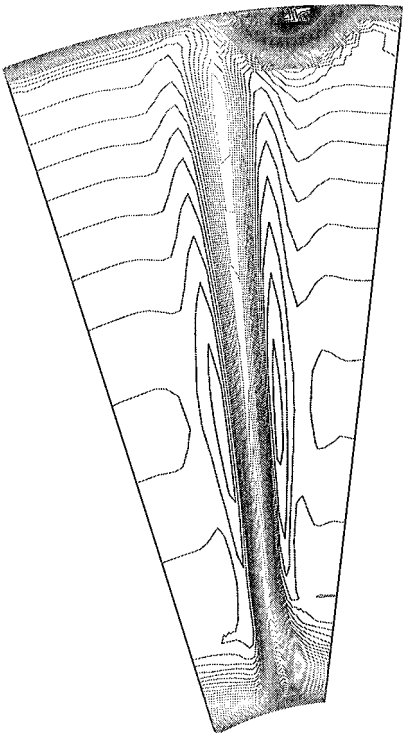

Figure 21. Mach number contours at VIGV exit.

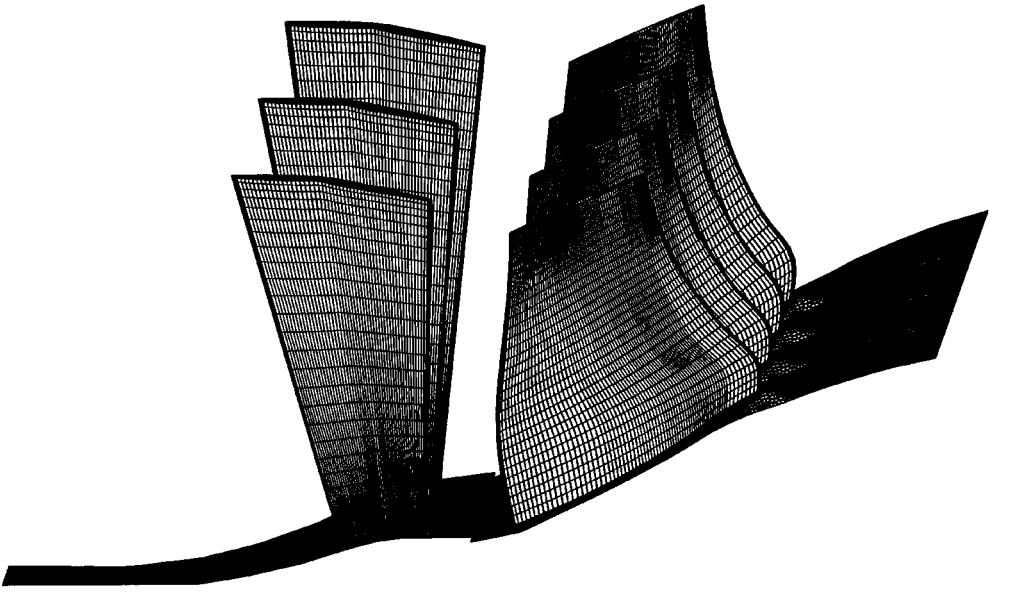

Figure 22. Multi-row mesh for forced response calculations.

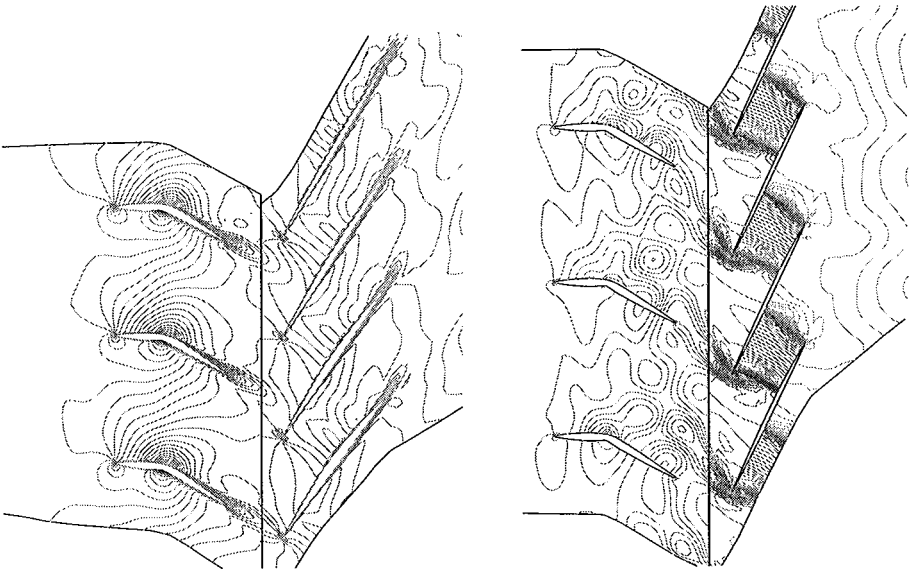

Figure 23. Instantaneous Mach number and pressure contours.

TABLE 2

Measured and predicted peak-to-peak vibration amplitudes for fan forced response

Case	Predicted amplitude (% chord)	Measured amplitude (% chord)
5 ND/Blade mode-11 family	0·11	0·11
5 ND/Blade mode-12 family	0·90	1·16

are plotted in Figure 24(a, b) for the two resonant conditions. Finally, a comparison of the measured and predicted maximum response is given in Table 2.

5. CONCLUDING REMARKS

The following conclusions may be drawn from the work in Parts I and II of this study.

(i) The forced response prediction methodology of Part I has been applied to two industrial cases: an HP turbine and a rig fan. Most of the numerical studies have been conducted in a time-accurate fashion with a nonlinear viscous flow representation. In addition, structural flexibility was accommodated by moving the fluid mesh according to the structural motion. The results suggest that the methodology can be applied, with reasonable confidence, to demanding industrial cases. Although such analyses require large computational resources, they are expected to become part of the routine design process because of their unique ability to predict actual blade-vibration levels.

(ii) For the HP turbine, the major part of the forcing is observed to be due to the inviscid (potential) effects. This is caused by the fact that the oblique shocks extending downstream of the trailing edge of the stator blades interact with the rotor blades.

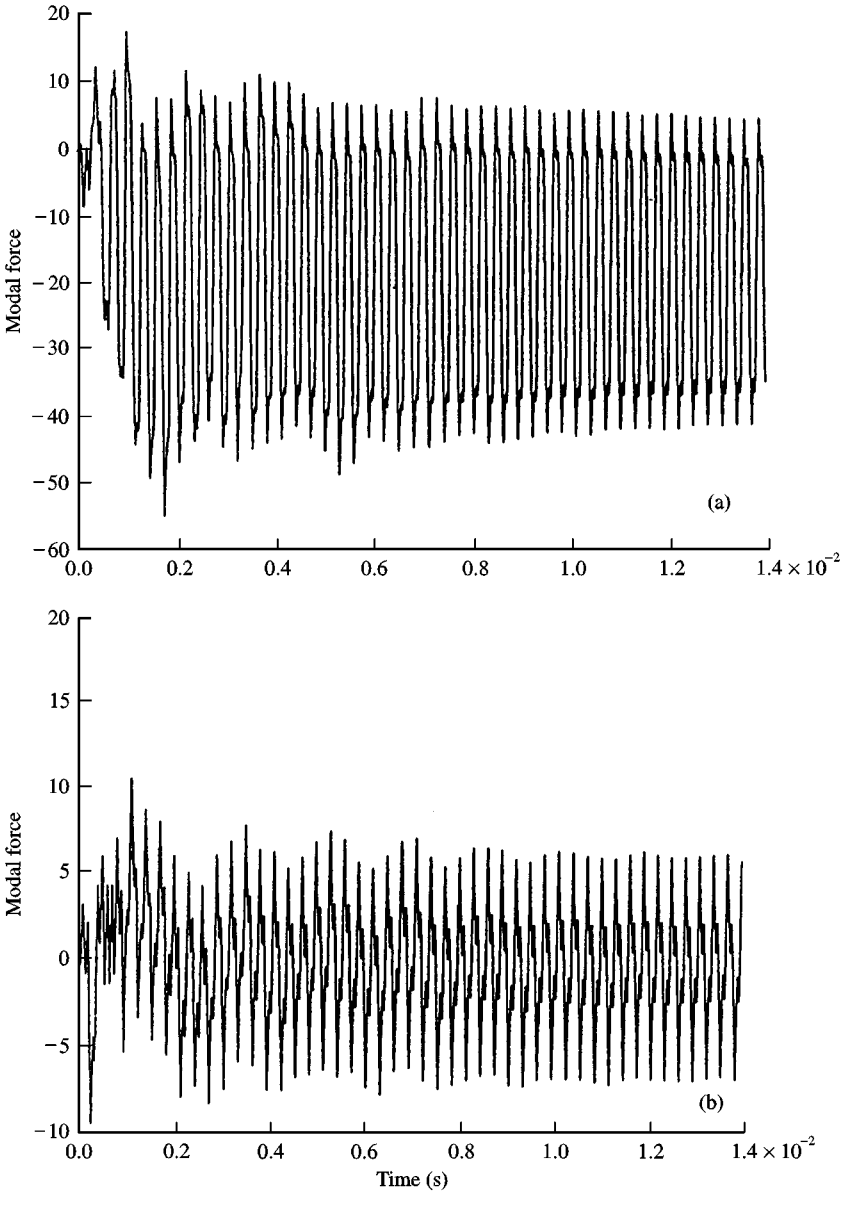

Figure 24. Modal force time history for (a) mode 11 and (b) mode 12.

(iii) The friction damping is predicted to reduce the peak-to-peak amplitude by about 30%. Similarly, the addition of two stator blades is seen to reduce the amplitude by about 5%.

(iv) Throat width variation is confirmed to be a source of low engine-order excitation. The unsteady aerodynamic forcing is predicted to increase in magnitude with increasing scatter in throat width variation.

(v) Given the uncertainties described in Section 1 of Part II, the accuracy of the forced response predictions is remarkably good. The main sources of error are expected to be the

assumed values of structural damping, friction damper modelling and simplifications in the aerodynamic modelling such as relatively coarse discretization, tip gap representation and omission of the hinge flow in the fan example. A further uncertainty is due to assembly mistuning which is likely to affect the measurements. Although readings from several strain gauges are averaged, the exact positions on the blade and the number of instrumented blades are thought to be significant factors.

(vi) Although the computations were performed in a coupled manner, the effects of fluid damping were found to be relatively small for both the turbine and the fan cases. However, blade flexibility may be a significant factor under some other operating conditions.

ACKNOWLEDGEMENTS

The authors would like to thank Rolls-Royce plc. for both sponsoring the work and allowing its publication. Some of the work was carried out with the support of the Ministry of Defence (MoD) and the Defence Evaluation Research Agency (DERA). They also thank Mr J. S. Green, Dr R. M. Hall, Mr S. J. Lee and Mr R. Elliott of Rolls-Royce for many very useful discussions. They also acknowledge the help of Drs Sanliturk and Bréard for the friction damper calculations.

References

Edmonds, J. D. *et al.* 1997 Recent developments in the application of Laser Doppler anemometry to compressor rigs. In *Symposium on Advanced Non-intrusive Instrumentation for Probulsion Engines*. AGARD.

Green, J. S. & Marshall, J. G. 1999 Forced response predictions within the design process. *In* 3*rd European Conference on Turbomachinery*, London, IMechE paper C557/067/99, pp. 377–391.

Sanliturk, K. Y. & Ewins, D. J. 1996 Modelling two-dimensional friction contact and its application using harmonic balance method. *Journal of Sound and Vibration* **193,** 511–523.

Sayma, A. I., Vahdati, M., Green, J. S. & Imregun, M. 1998 Whole assembly flutter analysis of a low-pressure turbine blade. 3*rd National Turbine Engine High Cycle Fatigue Conference*, San Antonio, Texas, U.S.A.

Sbardella, L., Sayma, A. I. & Imregun, M. 1997 Semi-unstructured mesh generator for flow calculations in axial turbomachinery blading. In 18*th International Symposium on Unsteady Aerodynamics and Aeroelasticity of Turbomachines* (ed. T. Fransson). Dordrecht: Kluwer Academic Publishers.

Sayma, A. I., Vahdati, M. & Imregun, M. 2000 An integrated nonlinear approach for turbomachinery forced response prediction. Part I: formulation. *Journal of Fluids and Structures* **14,** 87–101.